Int J Earth Sci (Geol Rundsch) (2013) 102:2097–2115
DOI 10.1007/s00531-013-0926-0

ORIGINAL PAPER

Episodic and long-lasting Paleozoic felsic magmatism in the pre-Alpine basement of the Suretta nappe (eastern Swiss Alps)

T. Scheiber · J. Berndt · B. D. Heredia · K. Mezger · O. A. Pfiffner

Received: 19 July 2012 / Accepted: 2 June 2013 / Published online: 28 June 2013

Abstract The Suretta nappe of eastern Switzerland contains a series of meta-igneous rocks, with the Rofna Porphyry Complex (RPC) being the most prominent member. We present LA-ICP-MS U–Pb zircon data from 12 samples representing a broad spectrum of meta-igneous rocks within the Suretta nappe, in order to unravel the pre-Alpine magmatic history of this basement unit. Fine-grained porphyries and coarse-grained augengneisses from the RPC give crystallization ages between 284 and 271 Ma, which either represent distinct magma pulses or long-lasting magmatic activity in a complex magma chamber. There is also evidence for an earlier Variscan magmatic event at ~320–310 Ma. Mylonites at the base of the Suretta nappe are probably derived from either the RPC augengneisses or another unknown Carboniferous–Permian magmatic protolith with a crystallization age between 320 and 290 Ma. Two polymetamorphic orthogneisses from the southern Suretta nappe yield crystallization ages of ~490 Ma. Inherited zircon cores are mainly of late Neoproterozoic age, with minor Neo- to Paleoproterozoic sources. We interpret the Suretta nappe as mainly representing a Gondwana-derived crustal unit, which was subsequently intruded by minor Cambrian–Ordovician and major Carboniferous–Permian magmatic rocks. Finally, the Suretta nappe was thrust into its present position during the Alpine orogeny, which hardly affected the U–Pb system in zircon.

Keywords Geochronology · Suretta nappe · Rofna Porphyry Complex · LA-ICP-MS · Zircon

Introduction

Within the Alpine continental collision zone of Europe, several pre-Alpine basement units are exposed that contain information about a variety of pre-Alpine magmatic and metamorphic events (e.g. Neubauer 2002; von Raumer et al. 2009; Bussien et al. 2011). Most of these pre-Alpine events can be assigned to two different orogenic cycles: (1) a Cambrian to Ordovician cycle (ca. 500–450 Ma; e.g. Guillot et al. 2002; Schaltegger et al. 2003) and (2) a Carboniferous to Permian cycle (the Variscan orogeny, ca. 350–270 Ma; e.g. Schaltegger 1997; von Raumer et al. 2009). The distribution and ages of these variable pre-Alpine magmatic and metamorphic events have been used to reconstruct the position of different pre-Alpine basement units within a Paleozoic to Mesozoic plate tectonic setting (e.g. von Raumer et al. 2009; Bussien et al. 2011).

The Suretta nappe, exposed in the eastern Swiss Alps, is one of several pre-Alpine Penninic basement nappes (Fig. 1). It hosts a suite of pre-Alpine meta-igneous bodies: in its northern part, the complexly deformed Rofna Porphyry Complex (RPC) contains coarse-grained gneisses with a typical augen texture (in the following termed augengneisses) and fine-grained porphyritic rocks. The coarse-grained fabric of the augengneisses suggests that they originated from plutonic rocks, whereas the fine-grained porphyritic rocks are interpreted to have a volcanic to sub-volcanic nature (Hanson et al. 1969; Milnes and

Electronic supplementary material The online version of this article (doi:10.1007/s00531-013-0926-0) contains supplementary material, which is available to authorized users.

T. Scheiber (✉) · B. D. Heredia · K. Mezger · O. A. Pfiffner
Institute of Geological Sciences, University of Bern,
Baltzerstrasse 3, 3012 Bern, Switzerland
e-mail: scheiber@geo.unibe.ch

J. Berndt
Institut für Mineralogie, Universität Münster,
Corrensstraße 24, 48149 Münster, Germany

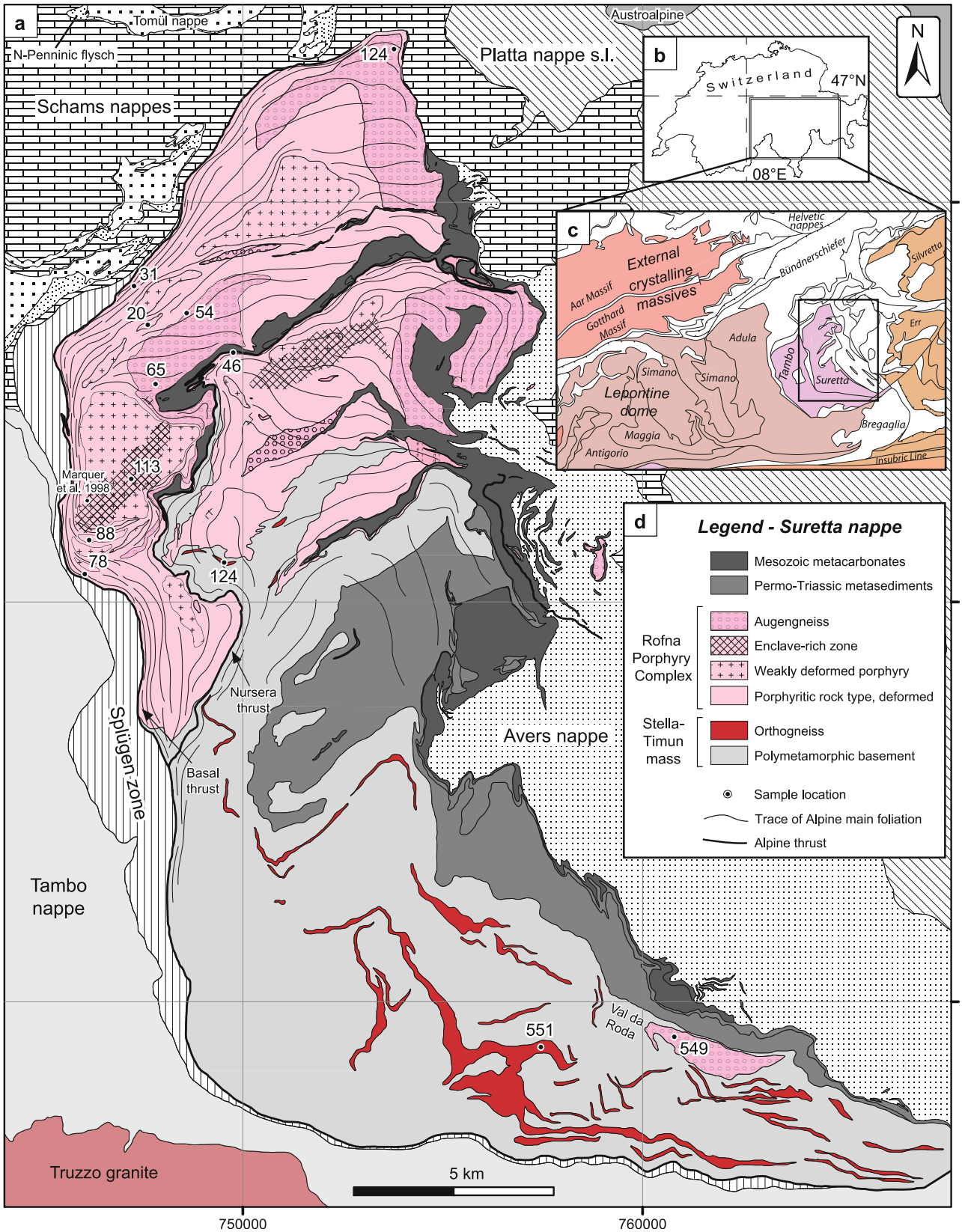
a
Tomül nappe
N-Penninic flysch
Austroalpine
Platta nappe s.l.
Schams nappes
124
31
20
54
65
46
113
88
78
124
Marquer et al. 1998
Nursera thrust
Basal thrust
Splügen zone
Avers nappe
Tambo nappe
551
549
Val da Roda
Truzzo granite
5 km
750000
760000
160000
150000
140000
b
Switzerland
47°N
08°E
N
c
Helvetic nappes
External crystalline massives
Aar Massif
Gotthard Massif
Bündnerschiefer
Silvretta
Err
Adula
Tambo
Suretta
Simano
Simano
Lepontine dome
Maggia
Antigorio
Bregaglia
Insubric Line
d
Legend - Suretta nappe
Mesozoic metacarbonates
Permo-Triassic metasediments
Rofna Porphyry Complex
Augengneiss
Enclave-rich zone
Weakly deformed porphyry
Porphyritic rock type, deformed
Stella-Timun mass
Orthogneiss
Polymetamorphic basement
Sample location
Trace of Alpine main foliation
Alpine thrust

◀ **Fig. 1** (**a**) Geological map of the Suretta nappe. Insets refer to (**b**) the location and (**c**) tectonic framework of the study area and to (**d**) the lithologies of the Suretta nappe. *Colored* units in (**b**) highlight the pre-Alpine basement units. The Tambo and Suretta nappes are part of the Briançon-derived continental crust. *Colored* units in (**a**) indicate meta-igneous rocks. The compiled geological map is based on maps of Staub (1926), Wilhelm (1929), Grünenfelder (1956), Streiff et al. (1971), Milnes and Schmutz (1978), Spicher (1980), Ganzfried (1984), Mayerat Demarne (1994), Marquer et al. (1998), Wiederkehr (2004), Berger and Mercolli (2006) and authors' own observations. Location of dated samples is provided by *black dots*. Alpine main foliation was traced where data are available

Schmutz 1978; Marquer et al. 1998). South of the RPC, several discontinuous tabular bodies of deformed granitic rocks (in the following termed orthogneisses) of various sizes occur within the polymetamorphic basement.

The age relationships between the various magmatic bodies exposed in the Suretta nappe are not entirely resolved. Hanson et al. (1969) presented age constraints from zircons from the RPC and suggested a minimum ($^{207}Pb/^{206}Pb$) age of emplacement of ~350 Ma, i.e., early Carboniferous. This age was revised by Marquer et al. (1998), who dated several multigrain zircon fractions from one porphyritic sample (Fig. 1): two nearly concordant fractions gave a mean $^{206}Pb/^{238}U$ age of 268.3 ± 0.6 Ma, suggesting a Late Permian intrusion age. The augengneisses within the RPC have generally been interpreted to be of Ordovician age (e.g. Spicher 1980; Marquer et al. 1996; Nussbaum et al. 1998), but geochronological data confirming this hypothesis are lacking so far. The age of the orthogneisses within the polymetamorphic basement of the southern Suretta nappe is unknown.

In this contribution, we present LA-ICP-MS (laser ablation inductively coupled plasma mass spectrometry) U–Pb zircon geochronological data from 12 samples covering various magmatic bodies from the entire Suretta nappe (Figs. 1, 2). We present the first age information for the orthogneisses in the south of the Suretta nappe and the first age information for the augengneisses within the RPC. We also present age information from the RPC porphyries, as well as from mylonitic rocks at the base of the nappe. These data help to reveal the nature and timing of magmatic events within this part of the pre-Alpine basement of the European Alps, and we discuss the results in the framework of the well-established Cambrian–Ordovician and Carboniferous–Permian orogenic cycles known from other pre-Alpine basement units in the Alps (e.g. Neubauer 2002; Schaltegger et al. 2003; Bussien et al. 2011).

Geological setting

The Suretta nappe is exposed in the eastern flank of the Lepontine structural dome in eastern Switzerland (Fig. 1). Together with the underlying Tambo nappe, it is part of the middle Penninic nappe system, which represents continental crust of the Briançon paleogeographic domain. Paleogeographic reconstructions for the Cretaceous (Stampfli et al. 1998; Schmid et al. 2004) reveal that the Briançon swell represents a piece of thinned European continental crust that separates two basins: the Piemonte–Liguria Ocean to the south and the Valais trough to the north. They are bordered by the continental margin domains of the Adriatic and European plates, respectively. The Suretta nappe contains several different rock units. (1) In the south of the Suretta nappe, a heterogeneous polymetamorphic assemblage, known as Stella-Timun mass or Timun complex, is mainly composed of paragneisses with amphibolite and orthogneiss lenses (Fig. 1; e.g. Milnes and Schmutz 1978). (2) The northern part of the Suretta nappe consists of a large, variably deformed igneous body, the Rofna Porphyry Complex (Fig. 1; Heim 1891; Wilhelm 1929; Hanson et al. 1969; Marquer et al. 1998; Scheiber et al. 2012). These rocks are described in more detail below. (3) The Stella-Timun and RPC rocks are overlain by and intercalated with an autochthonous to parautochthonous cover sequence, starting with discontinuous metatuffites, basal (Verrucano-type) conglomerates and white quartzites (Permo-Triassic), which are in turn overlain by Mesozoic carbonates (Fig. 1). The Permo-Triassic

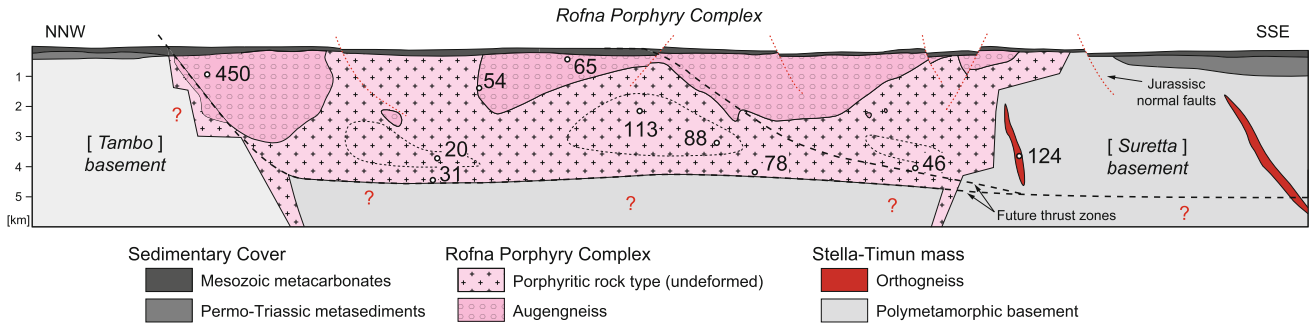

Fig. 2 Restored cross section showing the geological situation of the Rofna Porphyry Complex at the time of Jurassic rifting (modified after Scheiber et al. 2012). Augengneisses occupy a structurally high level within the RPC. Areas that resisted Alpine deformation are surrounded by *dashed lines*

sediments are thicker where they overly the polymetamorphic rocks of the Stella-Timun mass and very thin or even absent on top of the RPC.

The metamorphic and structural evolution of the Suretta nappe during the Alpine orogeny is relatively well understood. Thrusting and internal deformation took mainly place during two deformation phases in the middle Eocene: during the earlier Ferrera phase (c. 40–35 Ma), the nappe was thrust onto the underlying Tambo nappe and transported toward the NNW, whereas during the subsequent Niemet-Beverin phase (c. 35–32 Ma), backshearing and backfolding toward the S-SE took place (e.g. Milnes and Schmutz 1978; Marquer et al. 1996; Schmid et al. 1997; Scheiber et al. 2012). A restored cross section of the pre-Alpine situation is shown in Fig. 2. Metamorphism during the Alpine cycle reached upper greenschist facies conditions (Steinitz and Jäger 1981; Ring 1992; Nussbaum et al. 1998; Oberhänsli et al. 2004).

Geology of the Rofna Porphyry Complex and surrounding rocks

Traditionally, various rocks of magmatic origin have been distinguished within the RPC (e.g. Schmidt 1891; Rüetschi 1903; Grünenfelder 1956; Hanson et al. 1969; Streiff et al. 1976). However, in a recent study, Scheiber et al. (2012) distinguished mainly two types of meta-igneous rocks: porphyritic rocks and augengneisses (Fig. 1). According to Scheiber et al. (2012), the variable appearance of the magmatic rocks described by previous authors is mainly the result of a heterogeneous overprint by Alpine deformation. Fabrics in the porphyritic rocks range from undeformed or weakly deformed to mylonitic (Fig. 3a–d). With increasing deformation, the color changes from gray to green due to the appearance of abundant phengite.

About 80 % of the RPC consists of these variably deformed fine-grained porphyritic rocks (Fig. 1). They are composed mainly of rounded quartz and feldspar phenocrysts in an aphanitic matrix (Fig. 3a–b). Quartz grains are up to ~1 cm in diameter and many show corroded rims. Alkali feldspar augen reach the same size as quartz grains, whereas plagioclase and biotite are mostly finer grained and altered. In deformed porphyritic samples, biotite is generally absent. A more detailed description of the porphyritic rocks is given in Grünenfelder (1956), Gysin (1963), Hanson et al. (1969) and Marquer et al. (1998). They are generally interpreted as an acidic hypabyssal or subvolcanic intrusion (Hanson et al. 1969; Milnes and Schmutz 1978).

The porphyritic rocks intruded both the Stella-Timun mass and the augengneiss bodies of the RPC (Figs. 1, 2). The contact zone of the porphyritic rocks to the Stella-Timun mass is, in places, difficult to identify in the field, because of gneiss horizons within the polymetamorphic basement that look akin to foliated porphyritic rocks. The intrusive contacts between porphyritic rocks and augengneiss bodies are also poorly defined in the field. There is a transition zone of several meters to decameters wide, where the precursor of the augengneiss is apparently assimilated into the porphyritic rock. This assimilation may well be caused by magmatic assimilation and Alpine overprint. Furthermore, round blocks of augengneisses are observed within the porphyritic rocks close to the intrusive contact. In addition to these contact zones, abundant xenoliths were also observed within two domains of fine-grained porphyritic rocks in the interior of the RPC (Fig. 1). These xenoliths can be classified into four types: (1) Stella-Timun basement blocks, (2) blocks of RPC augengneiss, (3) leucocratic felsic enclaves of unknown origin, which are very common in the eastern zone (Fig. 3b and d) and (4) mafic microgranular enclaves (Fig. 3b). The latter two are often aligned within a magmatic foliation and may therefore present evidence for magmatic flow.

The remaining ~20 % of the RPC consists of augengneisses (Figs. 1, 3e). The augengneisses have the same mineralogical composition as the porphyritic rocks, but are, in contrast, coarser-grained (Fig. 3e). K-feldspars are up to 5 cm long, and quartz phenocrysts are usually larger than in the porphyritic equivalent (cf. Gysin 1963). Elongated masses of fine-grained sericite-rich aggregates define, together with the aligned K-feldspar and quartz augen, a penetrative schistosity. In many places, the augengneisses occur directly below Permo-Triassic sediments, but are never in contact with rocks of the Stella-Timun mass (Fig. 2). However, within the southern Suretta nappe, an isolated augengneiss body, akin to the RPC augengneisses, occurs within the Stella-Timun mass (Fig. 1). Furthermore, augengneisses of the RPC are always strongly foliated, in contrast to the variably deformed porphyritic rocks (Scheiber et al. 2012).

Rocks from the very base of the Suretta nappe were originally attributed to an "aphanitic border facies" of the RPC and interpreted as a sequence of tuffites and cinerites (Grünenfelder 1956; Hanson et al. 1969). However, in a recent study, Scheiber et al. (2012) interpreted these rocks as tectonically recrystallized fine-grained mylonites, probably developed from porphyritic rocks of the RPC, marking the basal thrust of the Suretta nappe (Fig. 3c). In these mylonites, fragments of K-feldspar phenocrysts (up to 3 mm in diameter) and even smaller quartz grains with long tails and fine-grained quartz-rich layers occur within the microcrystalline phengite-dominated matrix. A similar strongly deformed rock also occurs at the base of one major nappe-internal thrust fault, namely the Nursera thrust (Fig. 1).

South of the RPC, the Stella-Timun mass contains several orthogneiss bodies of various shapes and sizes (Fig. 1). The quantity of orthogneiss bodies increases toward the root zone of the nappe in the SE. These orthogneisses also contain deformed K-feldspar porphyroclasts and commonly have an augengneiss appearance, but they are much stronger deformed than the RPC augengneisses, richer in mica and generally have a darker color (Fig. 3f).

Analytical methods—LA-ICP-MS U/Pb dating

Zircons were separated using conventional magnetic and heavy liquid techniques followed by hand-picking using a binocular microscope. Individual grains were mounted in one-inch epoxy disks and polished down to roughly expose the grain centers. Before analysis, samples were characterized by backscattered electron (BSE) and cathodoluminescence (CL) imaging. The LA-ICP-MS analyses were

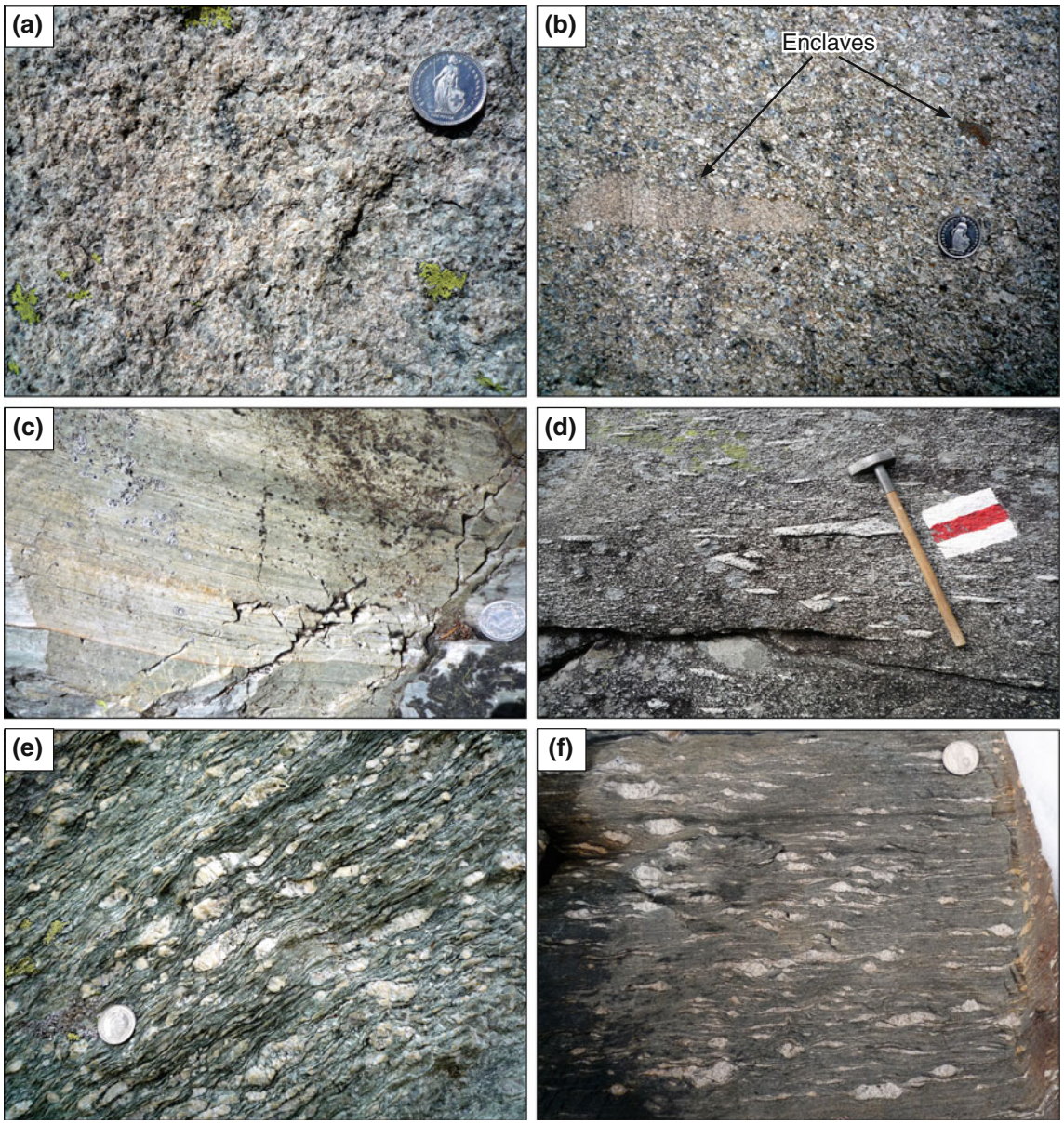

Fig. 3 Field aspect of various meta-igneous rocks from the Suretta basement. Swiss coordinates for each photograph are given. **a** Homogeneous, fine-grained and massive undeformed porphyry of the RPC (746158/151553). **b** Weakly deformed enclave-baring porphyritic rock type (746809/153016). **c** Mylonite from the basal thrust (746303/157064). **d** Enclave-rich, ignimbrite-like moderately deformed porphyritic rock (746809/153016). **e** Augengneiss facies of the RPC (748038/156138). **f** Orthogneiss within the polymetamorphic basement (749535/150992)

performed using a Thermo Finnigan Element 2 sector field ICP-MS coupled to a New Wave UP193HE ArF Excimer laser system at the Institut für Mineralogie, Universität Münster following the procedure of Kooijman et al. (2012). An in-house produced low-volume ablation cell following the design of Bleiner and Günther (2001) was used to reduce washout time and increase signal intensities.

Masses ^{202}Hg, ^{204}Hg + ^{204}Pb, ^{206}Pb, ^{207}Pb and ^{238}U were acquired in e-scan mode. ^{207}Pb/^{235}U was calculated from ^{207}Pb/^{206}Pb and ^{206}Pb/^{238}U using the natural abundance for ^{238}U/^{235}U (the "consensus value" of 137.88; Steiger and Jäger 1977). A laser spot size of 35 µm and, in some cases, 25 µm was used at energies of 5 J/cm^2 and a repetition rate of 10 Hz. The total ablation time per analysis was 52 s, including 15 s during which the shutter remained closed to measure the gas blank (i.e. background). Pre-ablation of all spots was done prior to analysis to remove common Pb from the surface. Laser-induced elemental fractionation and instrumental mass bias were corrected by bracketing groups of 10 unknowns with 3 analyses of GJ1 zircon as standard reference material (Jackson et al. 2004). Along with the unknowns, the 91500 standard zircon (Wiedenbeck et al. 1995, 2004) was measured to monitor precision and accuracy of the analyses. The external reproducibility was 2.5 % for ^{206}Pb/^{238}U and 3.0 % for ^{207}Pb/^{206}Pb (2σ).

Data were processed in an Excel spreadsheet following the procedure presented in Kooijman et al. (2012). A correction for common Pb (Stacey and Kramers 1975) was applied only if the estimated common ^{206}Pb of the total measured ^{206}Pb exceeded 1 %, because for samples with lower common ^{206}Pb contents, the total uncertainties of the resulting ages are by far dominated by the analytical uncertainties. In addition, for low amounts of common Pb, there is the risk of overcorrecting due to Hg interference. The complete analytical protocol and the correction procedures applied to the measured data are presented in detail in Kooijman et al. (2012). All errors are reported at the 2σ-level, and all uncertainties of multiple analyses are given as the 95 % confidence limit. The construction of concordia diagrams was performed using the ISOPLOT 3.71 program (Ludwig 2008). Single spot analyses are given as ^{206}Pb/^{238}U ages for results younger than 1 Ga and ^{207}Pb/^{206}Pb ages for results older than 1 Ga. All analytical data including the analyses of the zircon standard 91500 are reported in the supplementary data table. Only analyses with a degree of concordance more than 90 % were used for age calculations. All weighted mean ages were calculated using the ^{206}Pb/^{238}U ages and reported as 2σ confidence intervals. No discordia lines could be calculated for analyses that are less than 90 % concordant; discordant data might reflect multiple events that disturbed the U–Pb system.

Sample description and U–Pb LA-ICP-MS dating results

In order to resolve the age relationships between the different magmatic bodies observed in the Suretta nappe and in order to constrain the magmatic emplacement history of the RPC in more detail, we analyzed zircons from 12 samples representing the spectrum of igneous rocks hosted by this nappe. The samples belong to four groups: (1) weakly to undeformed porphyritic rocks (samples 20, 88, 113), (2) strongly deformed to mylonitic rocks (samples 31, 46, 78), (3) augengneisses (samples 54, 65, 450, 549) and (4) orthogneisses from the Stella-Timun mass (samples 124, 551). For sample location, see Figs. 1, 2 and Table 1. Wetherill U–Pb concordia diagrams are shown in Fig. 5, and ^{206}Pb/^{238}U weighted mean plots are provided for the Carboniferous–Permian record of the RPC rocks in Fig. 6. Zircon characteristics and the number of analyses are shown in Table 1. The complete LA-ICP-MS data of all samples are given in a supplementary data table.

Weakly deformed porphyritic rock type (RPC)

Sample 20 derives from a relatively small weakly deformed body of the RPC porphyry (Fig. 1). Sample 113 was taken from the central part of a large weakly to undeformed body within the RPC. The zircons analyzed by Marquer et al. (1998) come from a sample of the same igneous unit (Fig. 1). This unit hosts enclaves of variable size (up to 40 cm in diameter) and composition (Fig. 3b). Sample 88 is from another small and undeformed non-enclave-bearing body to the south of sample 113 (Figs. 1, 3a), which is surrounded by steeply dipping highly foliated porphyritic rocks. Zircon populations from all three samples are similar (Table 1). Most zircons contain xenocrystic, variably zoned cores, overgrown by one or several mostly oscillatory (low to highly luminescent)-zoned rims (Fig. 4a). Some zircons display moderately to highly luminescent, both oscillatory and planar zoned cores, which is typical of zircons precipitated during granite crystallization (e.g. Corfu et al. 2003).

Sample 20 One core was dated at 477 ± 14 Ma, and five core analyses together with nine rim analyses yield a weighted mean age of 271 ± 3 Ma (MSWD = 1.1) (Figs. 5a, 6a).

Sample 88 The >90 % concordant data (Fig. 5b) include four cores from four zircon grains. One spot gives a Neoproterozoic age of 634 ± 27 Ma (88_18, Fig. 4a); the three others correspond to bright magmatic cores, which are clustered together with spot analyses of 15 oscillatory-zoned rims. This cluster of 18 dates yields a concordant mean ^{206}Pb/^{238}U age of 275 ± 3 Ma (MSWD = 1.3) (Fig. 6a). The remaining spot 88_13 comes from a low

Table 1 Summary of sample locations, zircon characteristics and LA-ICP-MS analyses

Sample ID	Sample location Swiss grid coordinates		Rock type	Zircon characteristics			Analyses	
	Easting	Northing		Morphology	Size	Color	Number of analyses	Analyses >90 % concordant
20	747626	156938	Porphyritic rock type (RPC)	elongated, prismatic, euhedral	160–520 μm long, 70–140 μm wide	transparent, pink to brown	26	15
88	746158	151553					29	20
113	747209	153083					28	14
31	747281	157910	Mylonite (RPC)	euhedral to subeuhedral, commonly broken, fractured and corroded	70–380 μm long, 40–120 μm wide	transparent, colorless to pinkish	17	11
46	749763	156246					8	5
78	746048	150702					26	17
54	748596	157230	Augengneiss (RPC)	elongate to equant, euhedral	110–510 μm long, 70–140 μm wide	transparent, pink to brown	32	10
65	747819	155455					38	18
450	753782	163837					30	13
549	760789	139125					35	11
124	749535	150992	Orthogneiss (Stella-Timun mass)	elongate to equant, euhedral to subeuhedral, with slightly rounded outlines	180–360 μm long, 80–220 μm wide	transparent, pinkish	45	35
551	757456	138870					37	22

luminescent inner rim zone, which is truncated and overgrown by a 5 μm thin outer rim. It was dated at 303 ± 12 Ma.

Sample 113 Of the ages that are >90 % concordant, four analyses are from core areas. One yields a Neoproterozoic age of 642 ± 22 Ma (113_1, Fig. 4a), one has an Ordovician age (451 ± 16 Ma) and the two other analyses of bright magmatic cores plot in a cloud together with data obtained from nine oscillatory-zoned rims, giving a weighted mean age of 283 ± 3 Ma (MSWD = 0.4) (Figs. 5c, 6a). One inner oscillatory-zoned rim, which is unconformably truncated and overgrown by an outer rim (113_5, Fig. 4a), was dated at 320 ± 12 Ma.

Mylonites/Strongly deformed porphyry (RPC)

Samples 31 and 78 represent typical mylonites of the basal Suretta thrust (Figs. 1, 2), whereas sample 46 was taken from the nappe-internal Nursera thrust. All three samples contain considerably fewer zircons than samples of analogous size from the porphyritic rocks and augengneisses (Table 1). Many grains contain inherited cores, some with oscillatory zoning or, in rare cases, sector zoning typical of zircons of granitic origin (Fig. 4c). Some grains show resorbed, irregular outermost rims.

Sample 31 Six spot analyses within the >90 % concordant data (Fig. 5d) are from oscillatory-zoned rims of five crystals. One oscillatory-zoned rim was dated at 350 ± 9 Ma. Three spot analyses correspond to inner/intermediate rim areas (Fig. 4b) and point to an earlier crystallization at 328 ± 6 Ma (weighted mean $^{206}Pb/^{238}U$ age, MSWD = 0.4). Five rim measurements, together with two core analyses, yield a weighted mean age of 290 ± 7 Ma (MSWD = 3.1) (Fig. 6b). One spot (zircon 31_4) was dated at 261 ± 11 Ma.

Sample 46 One of the five analyses, which are more than 90 % concordant (Fig. 5e; Table 1), represents an inherited Neoproterozoic core (580 ± 13 Ma). Three analyses from differently textured zones give a weighted mean age of 289 ± 12 Ma (MSWD = 1.7), and one spot yields a date at 258 ± 7 Ma (Fig. 6b).

Sample 78 Within the >90 % concordant dataset, one analysis (19_1) represents a Neoproterozoic inherited core (651 ± 14 Ma). The rest of the concordant dataset yields Carboniferous–Permian ages between 310 and 263 Ma (Fig. 5f). One analysis of a core falls together with 11 points in low to highly luminescent oscillatory-zoned rims, giving a weighted mean age of 305 ± 2 Ma (MSWD = 1.1) (Fig. 6b). Another weighted mean age of 286 ± 4 Ma (MSWD = 1.0) can be obtained from three analyses of spots corresponding to three moderately luminescent oscillatory-zoned rims (e.g. 78_34, Fig. 4b). One highly luminescent outermost rim (78_20, Fig. 4b) was dated at 263 ± 7 Ma.

Augengneisses (RPC)

Samples 54 and 65 both belong to the same augengneiss body, which is exposed in the central part of the RPC. Sample 54 is located close to the contact with the

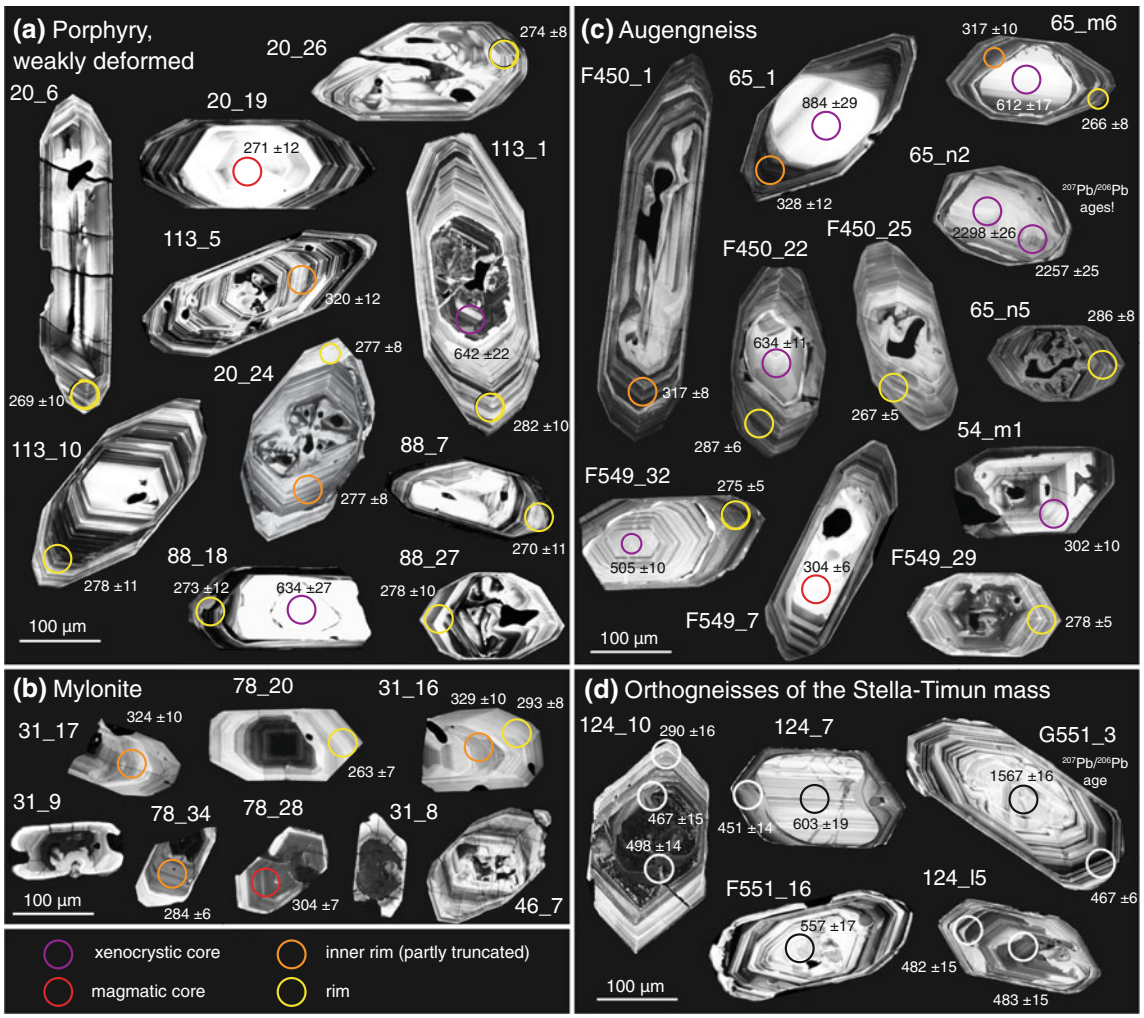

Fig. 4 Cathodoluminescence (CL) images of representative zircon crystals from meta-igneous rocks from the Suretta nappe. Scale is the same for all zircons. Analyzed spots are indicated by *circles* (diameter: 35 and 25 µm). *Color* scheme refers to the analyzed area within zircons from the RPC. Measured $^{206}Pb/^{238}U$ ages are provided, except for zircons 65n_2 and G551_3 $^{207}Pb/^{206}Pb$ ages are given

porphyritic rocks (Figs. 1, 2). Before Alpine thrusting, this body was most probably directly connected to the irregularly shaped augengneiss body in the east of the study area (Scheiber et al. 2012). Sample 450 comes from the upper part of the second large augengneiss body outcropping in the northeastern frontal part of the Suretta nappe (Fig. 1). One large augengneiss body exposed in the Val da Roda resembles the RPC augengneiss (Fig. 1; cf. Ganzfried 1984). Therefore, we mapped it as part of the RPC (Fig. 1), an interpretation, which is confirmed by the ages obtained from individual zircons in sample 549 (see below).

In all three samples, zircon rims exhibit regular magmatogenic oscillatory zoning. Zircon cores are either represented by xenocrysts of variable size and shape (Fig. 4c) or, more rarely, by oscillatory, low to highly luminescent domains having the same crystal shape and orientation as the surrounding rim. However, for some grains, CL imaging reveals more complex zoning with indications for local intermediate resorption. These inner rims show usually low luminescence, truncate highly luminescent oscillatory-zoned xenocrysts and are themselves truncated by an outermost oscillatory-zoned rim, which indicates resorption and subsequent overgrowth (zircons 65_1, 65_m6 and F450_1, Fig. 4c).

Sample 54 Three of ten >90 % concordant analyses (Table 1) are from inherited cores, yielding Mesoproterozoic (1,145 ± 70 Ma), Neoproterozoic (604 ± 21 Ma) and Devonian (393 ± 13 Ma) ages (Fig. 5g). Two oscillatory-zoned inner rims and one xenocrystic core (Fig. 4c, 54_m1) were dated at 315 ± 8 Ma, 302 ± 10 Ma and 281 ± 9 Ma. A population of four concordant ages around 268 ± 3 Ma (MSWD = 1.0) derives from oscillatory rim zones (Fig. 6c).

Sample 65 Two analyses (>90 % concordant) of one zircon core, which is surrounded by a thin euhedral rim

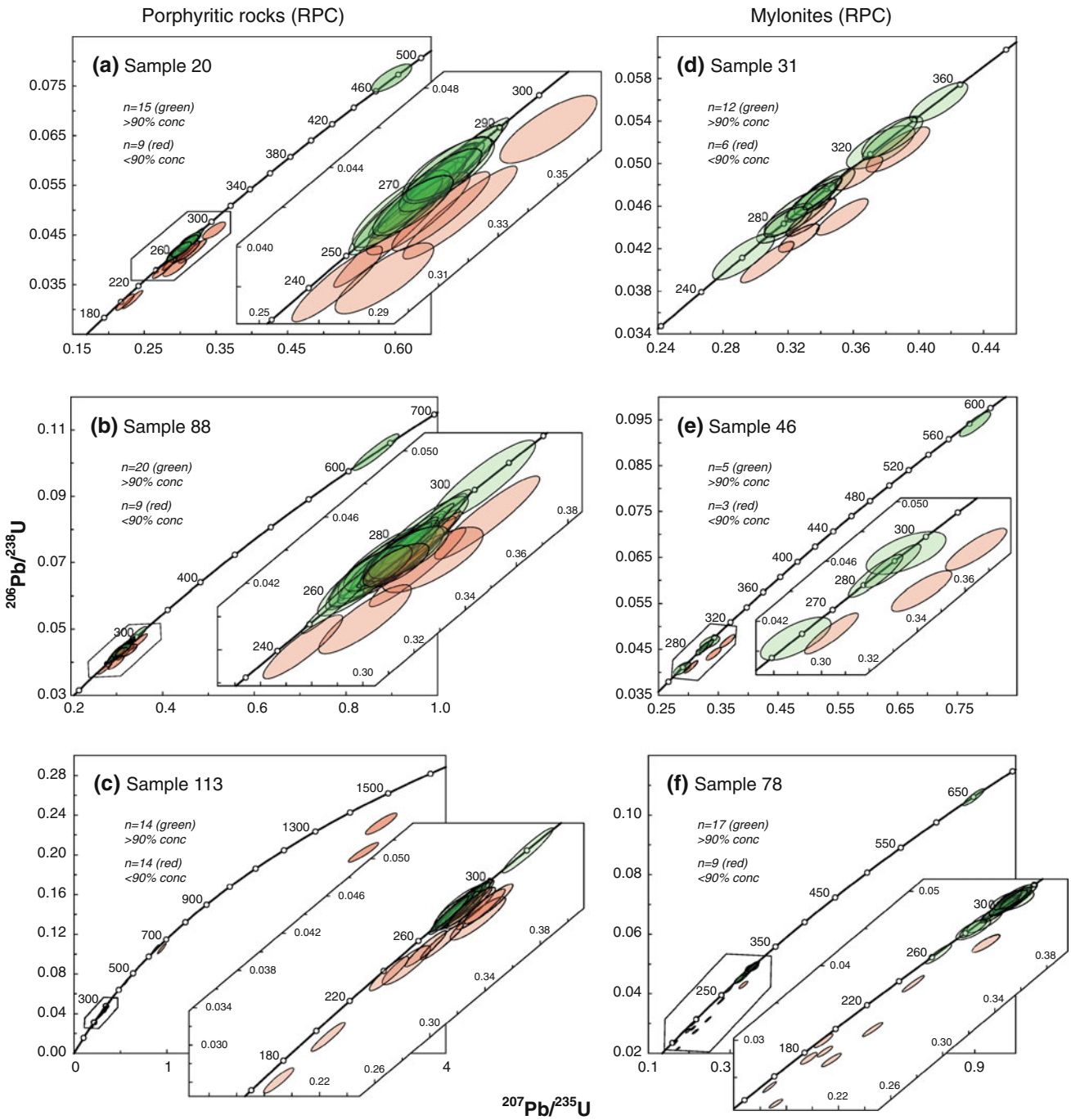

Fig. 5 Zircon U–Pb concordia plots for the studied samples from the Suretta nappe: **a–c** Weakly deformed porphyritic rock types (RPC). **d–f** Mylonites. **g–j** RPC augengneisses. **k–l** Orthogneisses of the Stella-Timun mass. Data more than 90 % concordant are shown with *green* ellipses, data more than 10 % discordant with *red* ellipses. Errors are reported at the 2σ-level

(65n_2, Fig. 4c) give Paleoproterozoic ages of 2,298 ± 26 Ma and 2,257 ± 25 Ma. There are three analyses of xenocrystic cores showing Neoproterozoic ages of 884 ± 29 Ma, 700 ± 23 Ma and 612 ± 17 Ma. The remaining analyses with >90 % concordance cover a broad time span of about 75 Ma between 328 ± 12 Ma and 251 ± 8 Ma (Fig. 5h). These results may indicate discrete age groups (Fig. 6c): Four spot analyses of inner rims and one core analysis indicate crystallization at 316 ± 10 Ma (weighted mean age, MSWD = 2.7). Another small group of three measured spots is from strongly oscillatory-zoned rim areas, which do not show any indications for resorption processes (e.g. 65_n5, Fig. 4c) and plot at ~285 Ma. The remaining analyses of outer rims and one magmatogenic

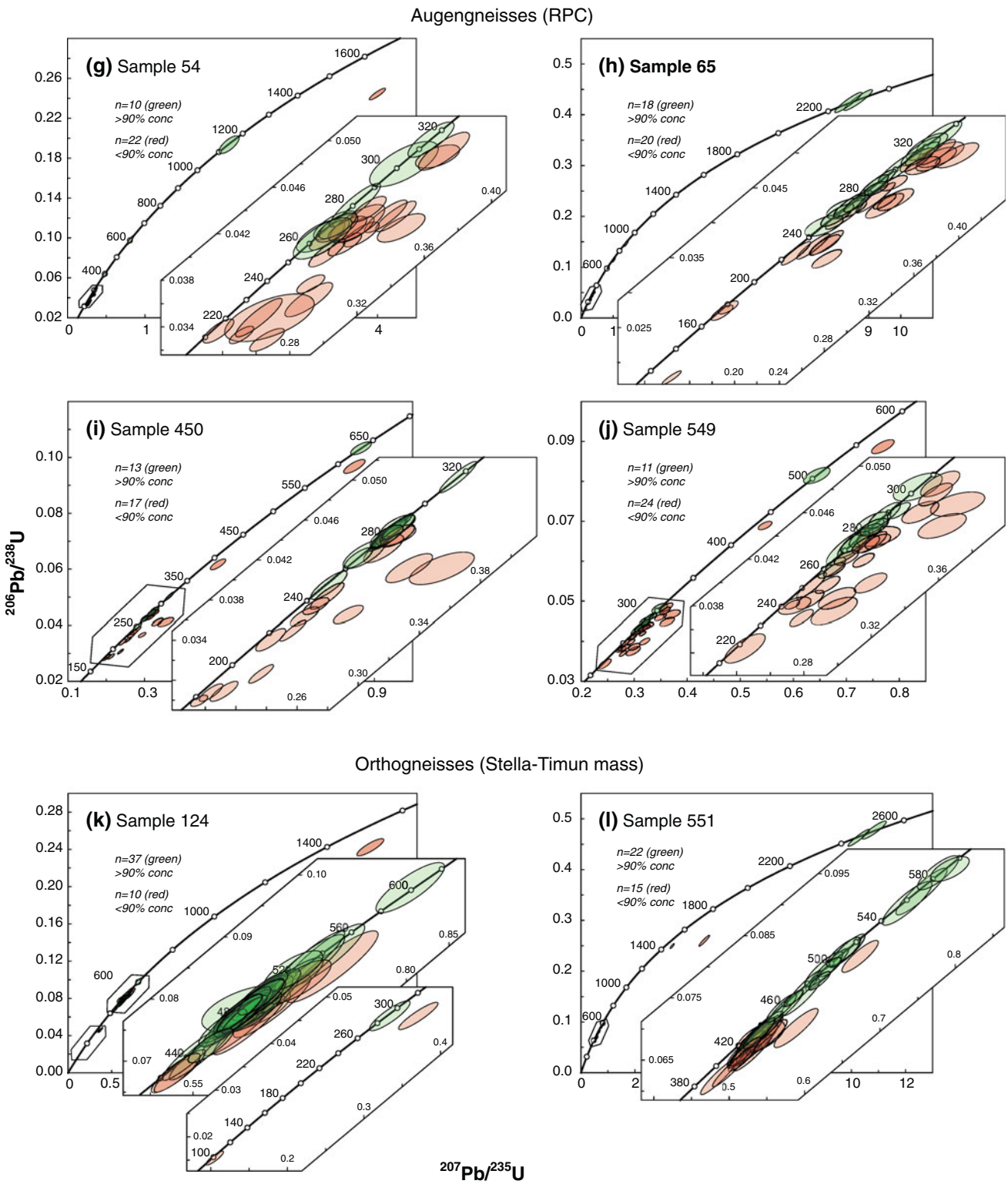

Fig. 5 continued

highly luminescent core deliver younger dates from ~270 to ~250 Ma (Fig. 6c).

Sample 450 One analysis from a central area of a sector-zoned moderately to highly luminescent xenocrystic core gives a Neoproterozoic crystallization age of 634 ± 11 Ma (F450_22, Fig. 4c). One inner low luminescent oscillatory-zoned rim, which was affected by resorption processes and is overgrown by another oscillatory rim, was dated at

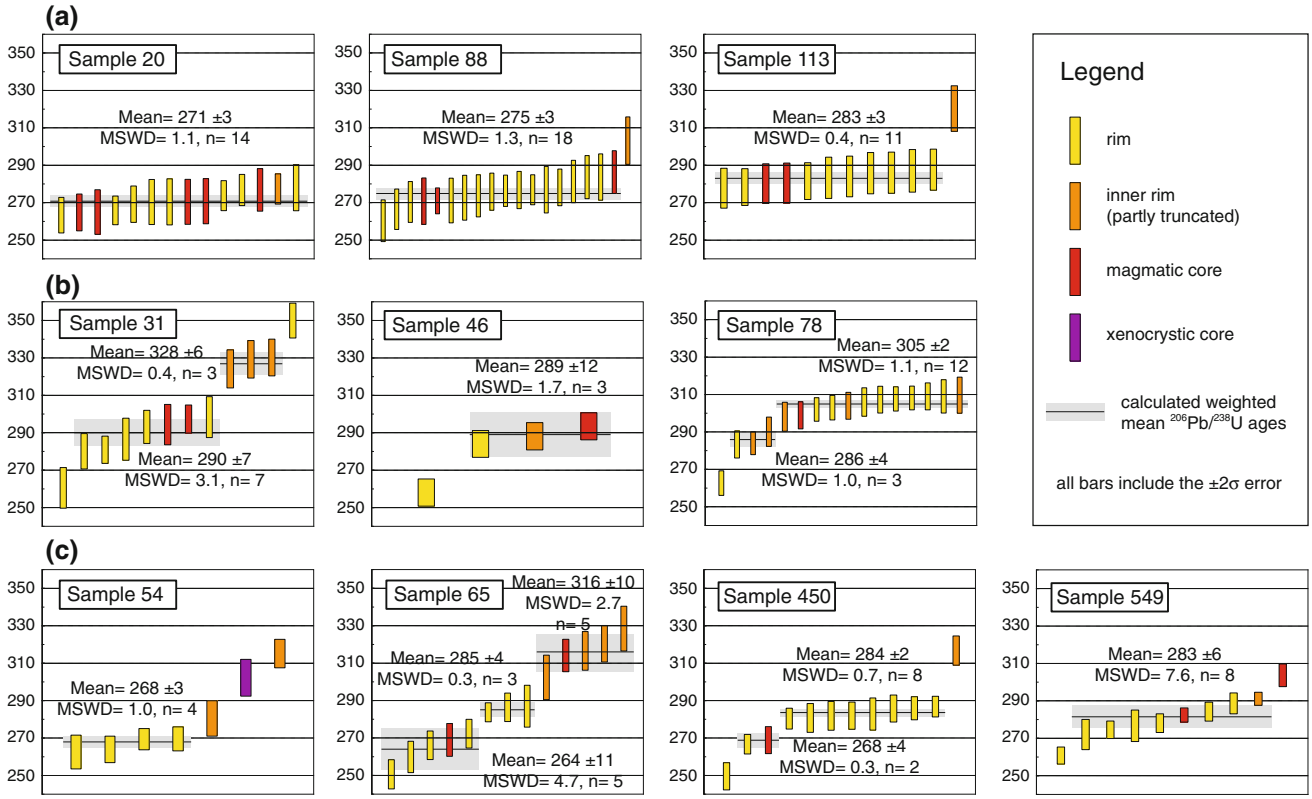

Fig. 6 $^{206}Pb/^{238}U$ weighted average plots of all Carboniferous–Permian ages (concordance >90 %) obtained from RPC (**a**) porphyritic rocks, (**b**) mylonites and (**c**) augengneisses. The origin of each spot analysis is indicated by the *color* scheme of the data bar (cf. *color* scheme presented in Fig. 4). For several zircon populations, the calculated weighted mean age is given

317 ± 8 Ma (F450_1, Fig. 4c). The contact between these two rims is marked by a high luminescent first section of the outer rim and indicates a round shape of the contact. Eleven spots from continuously oscillatory-zoned areas (ten rims and one core) yield ages below 300 Ma (Fig. 5i). Eight analyses give a weighted mean age of 284 ± 2 Ma (MSWD = 0.7), two scatter around 270 Ma and one was dated at 250 ± 7 Ma (Fig. 6c).

Sample 549 There is one inherited core yielding a Cambrian age of 505 ± 10 Ma. Two analyses from magmatic high luminescent cores and eight analyses from low to highly luminescent oscillatory-zoned rim areas range between 304 ± 6 and Ma 261 ± 5 Ma (Figs. 5j, 6c) with a concentration of ages around 283 ± 6 Ma (MSWD = 7.6).

Orthogneisses of the Stella-Timun mass

Samples 124 and 551 both derive from orthogneiss bodies within the Stella-Timun mass (Fig. 1) and are characterized by a light-gray color and a strong deformation state. They contain strongly altered K-feldspar phenocrysts (up to 4 cm in diameter) in a fine-grained matrix of mainly quartz, muscovite, K-feldspar, plagioclase and chlorite (Fig. 3f). Sample 124 was taken from a small orthogneiss body, which is close to the contact of the Stella-Timun mass to the RPC (Figs. 1, 3f). Sample 551 comes from a large orthogneiss body within the southern part of the Suretta nappe (Fig. 1).

Cathodoluminescence imaging revealed several inherited xenocrystic zircons, but also oscillatory magmatic cores occur (Fig. 4d). Cores are surrounded by low to highly oscillatory rims. These magmatic rims are commonly irregularly surrounded by an outermost highly luminescent up to 10 µm wide rim.

Sample 124 Within the concordant dataset, one analysis of an inherited core yields a Neoproterozoic age of 603 ± 19 Ma. Thirty-three analyses yield ages between 538 ± 25 Ma and 442 ± 20 Ma that correspond mainly to oscillatory-zoned rims and magmatic cores (Figs. 4d, 5k). However, this age distribution cannot be directly correlated with the internal structure of the zircon crystals (i.e. rims younger than cores). The weighted mean age for all 33 spot analyses is 487 ± 7 Ma (MSWD = 4.9). One Carboniferous–Permian age of 290 ± 16 Ma was obtained from a highly luminescent outermost rim (zircon 124_10, Fig. 4d).

Sample 551 There are three analyses of inherited cores dated at 2,498 ± 24 Ma, 2,460 ± 18 Ma and

1,567 ± 16 Ma (G551_3, Fig. 4d). Another set of four analyses of highly luminescent cores gives dates between 590 ± 10 Ma and 557 ± 17 Ma (Fig. 5l). Eleven of the fifteen remaining spot analyses show a $^{206}Pb/^{238}U$ age range from 512 ± 13 Ma to 457 ± 11 Ma giving a weighted mean age of 481 ± 12 Ma (MSWD = 13). The other four measurements giving the youngest dating results for this sample are only 90–93 % concordant and might therefore derive from the older age population by minor Pb-loss.

Discussion

The zircon textures and U–Pb ages from various intrusive rocks of the Suretta nappe allow a reconstruction of the pre-Alpine magmatic evolution of this tectonic unit. Clearly, the composite nature of the zircon grains, together with the wide scatter of U–Pb ages along concordia within each sample, is inconsistent with a simple magmatic history of this unit. The complex age patterns require a careful evaluation of the data combined with detailed investigation and comparison of the zircon textures and isotope composition.

Carboniferous–Permian zircon ages

The majority of the U–Pb analyses from (non-xenocrystic) cores, intermediate zones and rims of three weakly deformed porphyritic rocks, three mylonites and four RPC augengneisses are concordant between 350 and 250 Ma, i.e., Carboniferous–Permian in age (Figs. 6, 7). No concordant age younger than 250 Ma was obtained, and few inherited cores yielded Ordovician to Paleoproterozoic ages. This clearly shows that the augengneisses, previously interpreted as Ordovician or simply "older" intrusives, are of Carboniferous–Permian age and that the augengneiss body from the Val da Roda in the southern part of the Suretta nappe (sample 549) represents a member of the RPC as well. The RPC, therefore, represents a major composite Carboniferous–Permian magmatic complex. However, the details of this Carboniferous–Permian evolution are rather complex.

Spread of Carboniferous–Permian zircon ages

The concordant Carboniferous–Permian single spot analyses from the porphyries, mylonites and augengneisses are summarized in Fig. 6. The distribution of single analyses within the porphyritic rocks is "plateau-like" (Fig. 6a),

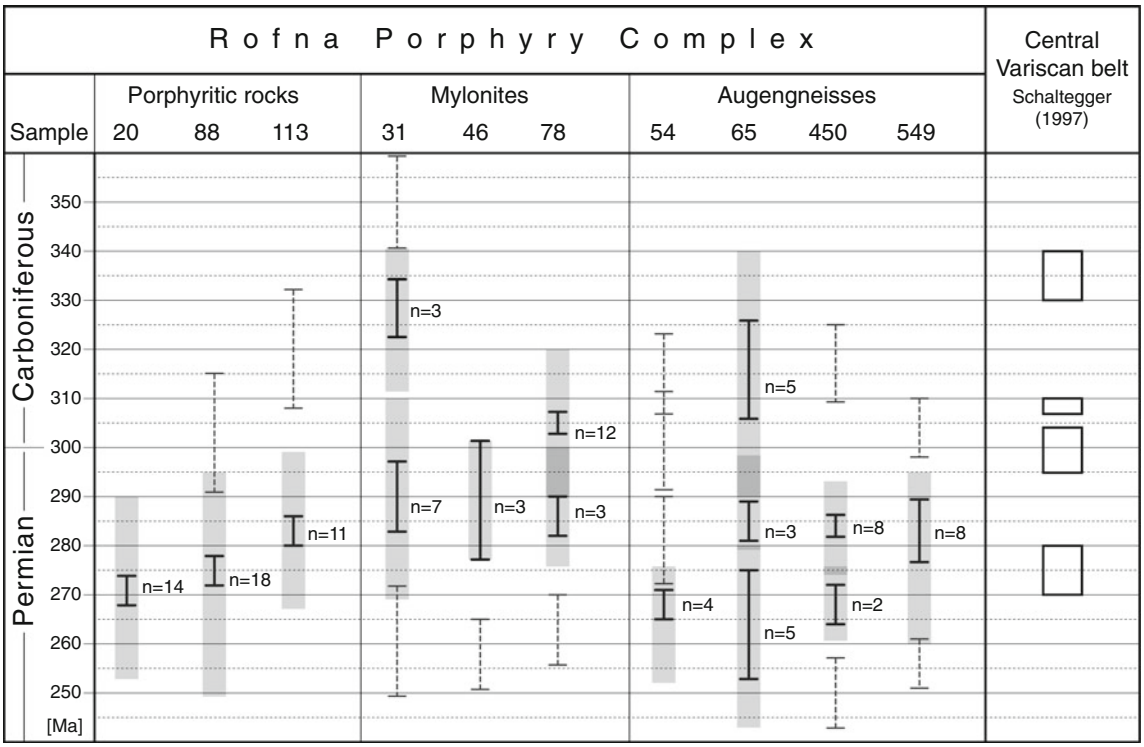

Fig. 7 Summary diagram of Carboniferous–Permian geochronological data for the RPC compared to late- to post-Variscan magmatic pulses within the Central Variscan Belt (Schaltegger 1997). For the RPC, ages are from more than 90 % concordant U–Pb data and are grouped according to rock types and samples. *Black bars* are keyed to calculated weighted mean ages (cf. Fig. 6), whereas *dashed bars* indicate single spot analyses. Bar height is equal to ±2σ error. Each *gray* background *bar* of a calculated age bar refers to the range from the youngest to the oldest spot analyses (±2σ error) included in the calculation

whereas the analyses in the mylonites (Fig. 6b) and augengneisses (Fig. 6c) show a "stair-case" pattern.

Such a dispersion in dates along concordia may be caused by (minor) Pb-loss (e.g. Mattinson 2005), incorporation of inherited zircon crystals (xenocrysts) or recycling of antecrysts sensu Miller et al. (2007). Antecrysts define a zircon crystal or a certain zone of it, which derives from earlier solidified or partially solidified magma inputs into the same magmatic system.

There are different approaches to interpret such age spreads along concordia. One way is to consider the oldest age population as representing the intrusion age, whereas all younger ages are interpreted to be the result of post-magmatic disturbance of the U–Pb system by recrystallization mainly due to fluid circulation coeval with and subsequent to the emplacement (e.g. Bomparola et al. 2007). In contrast, another commonly used approach (especially by the high precision TIMS community) is to consider the lower limit of a zircon concordia array to reflect zircon growth in the last increment of magma added to the system or complete quenching, which most likely approximates the age of intrusion (e.g. Miller et al. 2007; Schaltegger et al. 2009). By this consideration, older ages reflect inheritance of antecrystic or xenocrystic domains.

In the present case, incorporation of xenocrysts into the zircon spot analyses can be largely excluded since CL imaging combined with high spatial resolution of the LA-ICP-MS method provides control over the analyzed zircon fraction. The more challenging part is the influence of Pb-loss. In general, if Pb-loss is the predominant factor for age spread, it is expected that the data points do not lie on concordia. However, with relatively big error ellipses on single analyses, and only minor curvature of the concordia curve in the area of interest, some Pb-loss could be hidden within the concordant dataset. Therefore, some of the youngest ages within this dataset may be the result of Pb-loss due to younger post-crystallization thermal events. Common Pb as a cause for the age spread can be excluded, because this would lead to systematically reversely discordant data, which is not observed in our dataset. Consequently, the concordant age spread over such a long time span as present in our data cannot be explained by analytical reasons and cannot be interpreted as the result of Pb-loss only but may correspond, at least partly, to a real spread in zircon crystallization ages.

Porphyritic rocks

Single spot analyses within each of the three porphyritic rock samples show relatively little spread, and weighted mean ages of 271 ± 3, 275 ± 3 and 283 ± 3 Ma can be calculated for the different samples if two clearly older analyses within samples 88 and 113 are excluded (Figs. 6a, 7). The significance of these three calculated weighted mean ages has to be interpreted with care, since the error bars of the single spot analyses from all three samples overlap. There are two possible interpretations for these data: (1) If all three samples crystallized simultaneously from the same batch of magma, all analyses have to be taken together, and the mean age of ALL analyses (i.e. 275 ± 2 Ma, MSWD = 1.7, $n = 43$) most closely approximates the time of intrusion. Notably, this mean age is 7 m.y. older than the intrusion age (TIMS analyses) derived for the same porphyritic rocks by Marquer et al. (1998; 268.3 ± 0.6 Ma). (2) The other interpretation is that the three different mean ages of the three different samples indeed represent different crystallization ages. In this case, the porphyritic rocks of the RPC would be the result of several pulses of magma spread over 6–14 m.y. (Fig. 7). However, field evidence for different generations of porphyritic rocks intruding each other has not been observed.

Two clearly older zircon ages in samples 88 and 113 (303 ± 13 and 320 ± 12 Ma) are derived from low to moderately luminescent oscillatory-zoned areas, which truncate an inherited core and are themselves irregularly overgrown by an outer oscillatory-zoned rim (e.g. Fig. 4a; zircon 113_5). Analyses with similar ages are more abundant in the mylonitic and augengneiss samples (Figs. 6, 7) and might represent an earlier pulse of magmatism as discussed below.

Augengneisses

The augengneisses are clearly crosscut by porphyritic rocks, and consequently, have to be older (Figs. 1, 2). However, interpreting the different spot analyses from the augengneisses in terms of intrusion age is difficult. Three out of the four augengneiss samples show age clusters around 284 Ma, with weighted mean ages of 285 ± 4, 284 ± 2 and 283 ± 6 Ma (Figs. 6c, 7). The fourth sample (54) also shows one analysis within this range. In addition to these clusters, younger and older ages are present. The younger ages overlap with the main clusters from the porphyritic rocks, and the older ages have a spread between ca. 290 and 330 Ma, similar to the two older analyses in the porphyritic rocks (Fig. 7). The older ages all come from cores or inner rim areas (Figs. 4c, 6c).

There are again at least two interpretations possible for these data: (1) The clusters around 284 Ma could represent the crystallization age of the magmatic precursor of the augengneiss bodies. Younger ages could be the result of disturbance of the U–Pb system during later processes, probably during the magmatic activity associated with the emplacement of the porphyritic rocks. (2) Alternatively, the zircon age distribution within the augengneisses could be the result of complex protracted magma accumulation and

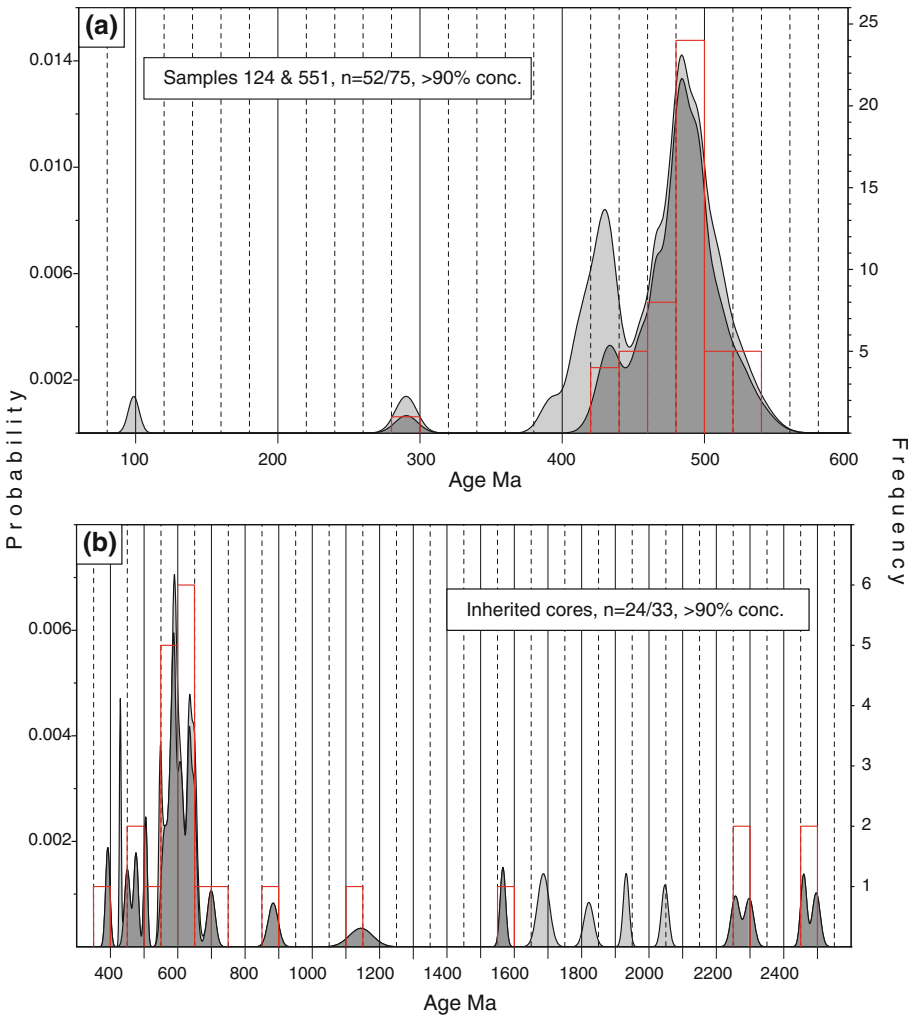

Fig. 8 Illustration of combined diagrams including *probability density plots* and *frequency histograms* of $^{206}Pb/^{238}U$ ages for (**a**) orthogneisses of the Stella-Timun mass and (**b**) all ages obtained from xenocrystic cores. *Plots* were created using the Excel worksheet presented by Sircombe (2004). *Darker* shaded probability density diagrams indicate age distribution of concordance-filtered data at 90–110 %. Histogram data were also filtered at this level. *Lighter* shaded probability density diagrams include all data. A bin width of 20 Ma was used for the Cambrian–Ordovician ages of sample 124 and 551, and 50 Ma for the analyses of inherited cores

zircon crystallization over a long time span within a deeper crustal level, before the final emplacement and solidification that is recorded by the youngest zircon population. These youngest zircon populations show similar weighted mean ages as the porphyritic rocks (e.g. 268 ± 3, 264 ± 11 and 268 ± 4 Ma, Fig. 6c), which would mean that the final emplacement of the augengneisses and porphyritic rocks was only separated by a very short, not resolvable time span.

The zircon age spectra from augengneisses exhibit, in contrast to those from porphyritic rocks, more discordant ages (Fig. 5), which is in agreement with the more strongly deformed state of the augengneisses relative to the weakly deformed porphyritic rocks. However, no discordia line could be calculated, which points to multiple events disturbing the U–Pb system, one of them possibly being the Alpine thrusting event.

Mylonites

The distribution of the zircon dates obtained for the mylonites is equally difficult to interpret (Figs. 6b, 7). One of the main questions regarding the mylonites has always been their protoliths (e.g. Vocke et al. 1987; Dickin 1988; Scheiber et al. 2012). Zircons from sample 46, taken at the Nursera thrust, yield four concordant ages, which fit the populations observed in the augengneisses (Fig. 7). Since the protolith is no more recognizable due to high strain, and since the Nursera thrust is a broad mylonitic zone, it is possible that the analyzed rock derives from a strongly deformed relic of an augengneiss body. The protolith of mylonites from the basal thrust (sample 31 and 78) remains also enigmatic due to strong mylonitization. Previous studies proposed a porphyritic rock as protolith (Hanson et al. 1969; Vocke et al. 1987; Scheiber et al. 2012), but the geochronological data do not necessarily support this interpretation. In contrast, the 271–283 Ma age cluster represented by the weakly deformed porphyritic rock is generally lacking in the age range obtained from the mylonites (Figs. 6, 7). The age spectrum of sample 31 largely matches clusters in the augengneisses, whereas sample 78 contains a cluster with an age of 305 ± 2 Ma, which is absent in both the porphyritic and augengneiss

samples (Fig. 6b). These data suggest that the mylonites probably either are derived from an augengneiss protolith or had a totally different magmatic precursor.

The geochemical characteristics of undeformed versus recrystallized (mylonitic) rocks of the RPC show that the mylonitic rocks are enriched in heavy rare earth elements over the light rare earth elements (Hanson et al. 1969; Vocke et al. 1987; Dickin 1988). Vocke et al. (1987) state that recrystallization happened isovolumetrically, but coincided with major mobilization of light REE, whereas Dickin (1988) concluded that the mylonite underwent 50 % volume loss during tectonism associated with a catastrophic loss of major elements and moderate loss of light REE. However, these interpretations are no longer appropriate if another rock was the protolith of the mylonite.

Another interesting feature is the influence of mylonitization on the zircons and their U–Pb systematics. Zircons from the mylonites are generally smaller than zircons from less deformed rocks and are commonly broken. Furthermore, radial and crosscutting microfractures were observed (Fig. 4b; e.g., zircons 31_8, 31_9 and 46_7), which is a common feature of radiation damage by alpha-decay predisposing brittle failure during ongoing shear stress (Wayne and Sinha 1992). Some zircons show resorbed outer boundaries (Fig. 4b, e.g., zircons 31_9 and 31_17), which could be the result of fluids present during mylonitization.

The influence of this deformation onto the U–Pb system of the zircons is more difficult to evaluate. A few analyses were performed on microfractured zircons from the mylonites. They gave no meaningful results because of unstable signals and/or high common Pb and are therefore not reported in the data tables and figures. This suggests that the U–Pb system of the most severely fractured zircons also was highly disturbed by the deformation, preventing any meaningful age determination. Nevertheless, many less fractured grains allowed age determinations (Figs. 5, 6), and these ages seem not to be severely disturbed by the Alpine deformation relative to the ages derived from less deformed porphyritic rocks and augengneisses (Figs. 5, 6). The discordant ages from the mylonitic samples allow no simple discordia line calculation with an Alpine lower intercept age, which would indicate Pb-loss during Alpine shearing. In addition, there are no observations of zircon overgrowths with Alpine age. These observations together indicate that Alpine mylonitization under upper greenschist facies conditions only caused disturbance of the U–Pb system in the most severely fractured grains—the U–Pb system of the majority of zircon grains within these mylonites was not affected by Alpine shearing. This in turn implies that Alpine thrusting along the basal and Nursera thrust of the Suretta nappe was a rather dry and fast process where grain-size reduction was the dominant process and not the growth of new minerals.

Significance of the Carboniferous–Permian ages in the context of the Variscan orogeny

The time span of 350–250 Ma corresponds to the construction and destruction of the Variscan orogen in central Europe (e.g. Franke 2006). Remnants of Variscan magmatism are widespread all over Europe and are generally attributed to several extensional phases, which readjusted the thickened continental lithosphere during and subsequent to the Variscan orogeny (Schaltegger 1997; Wilson et al. 2004; Franke 2006; Marotta and Spalla 2007; Kroner et al. 2008; Schuster and Stüwe 2008; Timmerman 2008; and references therein). In basement units within the Alps, late- to post-Variscan granitoids are volumetrically less important compared to their northern foreland, for example, in the nearby Black Forest or the Vosges (Eisbacher et al. 1989; Pfiffner 1993; Finger et al. 1997; Schaltegger 2000; Hann et al. 2003). Within basement units attributed to the Briançon domain, Variscan magmatic rocks of similar age to the RPC occur for example in the Tambo nappe (Truzzo granite, Marquer et al. 1998) or within the Siviez-Mischabel nappe (Randa orthogneiss, Thélin et al. 1993). These bodies are all relatively small and isolated intrusions, different from the large Variscan batholiths from the external crystalline massifs of the central and western Alps or the intrusions in the northern foreland.

Similarly to the different size and nature of the Variscan intrusives within the Alpine nappes relative to the foreland, the timing of the Variscan intrusions within the Alpine nappes seems to be slightly different from the timing in the foreland. Late- to post-Variscan magmatic pulses for the time intervals 340–330 Ma, 310–307 Ma, 304–295 Ma and 280–270 Ma were established for the Central Variscan Belt by Schaltegger (1997). The age spectrum observed within the present study does not fit well into this scheme (Fig. 7). However, the existence of a similarly complex long-lived granitoid magma system has recently been reported from the NE part of the Variscan Belt (e.g. Kryza et al. 2012), and the most abundant ages within the RPC can be correlated with results from a series of magmatic bodies in basement units from the southern Alps (e.g. Schaltegger and Brack 2007), the eastern Alps (e.g. Eichhorn et al. 2000) and the central and western Alps (e.g. Bonin et al. 1993; Bertrand et al. 2000b; Bussy et al. 2000).

Cambrian–Ordovician magmatism

Zircons from orthogneiss bodies within the Stella-Timun mass (samples 124 and 551) yield concordant Cambrian–Ordovician ages that scatter around 490 Ma (Fig. 8a). Such ages occur in the Alps (Neubauer 2002; von Raumer et al. 2002, and references therein) and are distributed over Western Europe, from Iberia (e.g. Díez Fernández et al.

2012) and France (e.g. Ballèvre et al. 2012) to the Bohemian Massif (e.g. Pin et al. 2007). This age frame corresponds to magmatic activity associated with the continental breakup of Gondwana, particularly rifting processes along the north-Gondwana margin (e.g. von Raumer et al. 2002, 2003; Galli et al. 2012). In the central and western Alps, igneous rocks dated at ~490 Ma (Cambrian–Ordovician boundary) are prevailing in Briançon-derived basement units: the Stella-Timun orthogneisses are in the same age range as intrusive rocks hosted by the Bernard nappe complex (Bussy et al. 1996; Bertrand et al. 2000a). Younger (Ordovician) intrusions (between 480 and 450 Ma) can be found in Briançon basement (Bertrand et al. 2000b; Guillot et al. 2002), but also in other basement units of the Alps (e.g. Schaltegger and Gebauer 1999; Schaltegger et al. 2003; Bussien et al. 2011). These granitoid intrusions are in turn interpreted as the result of crustal thickening during an Ordovician orogenic cycle (e.g. Schaltegger et al. 2003).

Age of inherited zircons

Xenocrystic zircon cores from both Cambrian–Ordovician and Carboniferous–Permian igneous rocks preserve ages ranging from 2.5 Ga to 400 Ma (Fig. 8). They indicate inheritance from different magmatic or metamorphic events. Ages around 600 Ma are the most prominent ones and probably represent a signature from the Neoproterozoic assembly of Gondwana. Zircons with such ages are fairly common in orthogneisses of the Variscan Belt (e.g. Oberc-Dziedzic et al. 2003). Locally, intrusions of this age are present in pre-Alpine basement nappes (e.g. Schaltegger et al. 1997; Korokovsky et al. 1998).

The ~490 Ma intrusion age recorded in the zircons from the orthogneisses of the polymetamorphic basement of the Suretta nappe occurs only rarely in the age spectra obtained from inherited cores. This implies that these orthogneisses were only a minor source and/or host rock of the RPC. Furthermore, there is limited evidence for other Neo-, Meso- and Paleoproterozoic events (Fig. 8b).

Conclusions: constraints for a model of the crustal evolution of the Suretta nappe

LA-ICP-MS dating of various magmatic rocks from the Suretta nappe of eastern Switzerland revealed the following history for the crustal evolution of this nappe:

1. Inherited zircon cores of mainly late Neoproterozoic age provide evidence that the Suretta nappe consists of material generated predominantly during the assembly of Gondwana. Minor contributions from older crustal sources as old as 2.5 Ga are also evident.
2. This crustal material was then the source of magmas that intruded as minor upper Cambrian to lower Ordovician (ca. 490 Ma) granitic rocks, possibly related to rifting and continental breakup (e.g. Neubauer 2002; Pin et al. 2007).
3. The majority of magmatic rocks of the Suretta nappe are the products of various crystallization events associated with the Carboniferous to Permian Variscan orogeny, including the augengneisses, which previously were interpreted as Ordovician or older rocks.
4. Ca. 320–310 Ma old zircons represent an early phase of Carboniferous magma crystallization, which clearly predates the major production of granitic magmas at 284–271 Ma. The oldest Carboniferous–Permian age population at around 315 Ma may therefore represent a relic of an intrusion, which was emplaced at this time and, later on, served as the source rock for the incremental formation of the RPC itself.
5. Small metamorphic overgrowths on Cambrian–Ordovician zircons from the southernmost orthogneisses within the Suretta nappe crystallized at ca. 290 Ma, when magmatic rocks of the RPC started to form. This suggests that the pre-RPC basement of the Suretta nappe was metamorphosed under high-grade conditions (cf. Nussbaum et al. 1998) at ca. 290 Ma and, furthermore, that considerable exhumation must have had occurred before the onset of subvolcanic activity, including the emplacement of RPC porphyries at 283–271 Ma.
6. The main formation of magmatic rocks within the RPC occurred between 284 and 271 Ma, either as distinct pulses or as prolonged and complex processes within a long-lasting magma chamber. This implies that the geodynamic setting at late- to post-Variscan times enabled long-lasting magmatism at more or less the same place and that the RPC, despite its relatively simple appearance in the field, might represent a complex composite magma chamber.
7. Mylonites from the basal thrust seem to have other protoliths than previously assumed. This is consistent with the difference in the REE signature of these rocks compared to undeformed RPC porphyries, observed by Vocke et al. (1987). Strain along the basal thrust of the Suretta nappe may have been localized along primary heterogeneities, where the protolith of the mylonite represented a weak zone compared to the porphyritic rocks.
8. Despite considerable Alpine deformation of the mylonitic rocks, only minor disturbance of the zircon U–Pb isotopic systematics is evident, and no zircon growth that can be related to the Alpine orogeny is observed.

Acknowledgments The authors thank Ivan Mercolli and Deta Gasser for fruitful discussion and Wolf-Christian Dullo for the careful editorial handling of the manuscript. The constructive reviews of Tom Andersen and Ryszard Kryza greatly improved the paper. This project was funded by the Swiss National Science Foundation (Grant no. 200020–122143).

References

Ballèvre M, Fourcade S, Capdevila R, Peucat JJ, Cocherie A, Fanning CM (2012) Geochronology and geochemistry of Ordovician felsic volcanism in the Southern Armorican Massif (Variscan belt, France): implications for the breakup of Gondwana. Gondwana Res 21(4):1019–1036

Berger A, Mercolli I (2006) Tectonic and Petrographic map of the Central Lepontine Alps, Sheet 43 Sopra Ceneri. Spezialkarte 127. swisstopo, Wabern

Bertrand JM, Guillot F, Leterrier J (2000a) Âge Paléozoique inférieur (U-Pb sur zircon) de métagranophyres de la nappe du Grand-Saint-Bernard (zona interna, vallée d'Aoste, Italie). Comptes Rendus de l'Académie des sciences Series IIA Earth and Planetary Science 330(7):473–478

Bertrand JM, Pidgeon RT, Leterrier J (2000b) SHRIMP and IDTIMS U-Pb zircon ages of the pre-Alpine basement in the Internal Western Alps (Savoy and Piemont). Schweiz Mineral Petrogr Mitt 80(3):225–248

Bleiner D, Günther D (2001) Theoretical description and experimental observation of aerosol transport processes in laser ablation inductively coupled plasma mass spectrometry. J Anal At Spectrom 16(5):449–456

Bomparola RM, Ghezzo C, Belousova E, Griffin WL, O'Reilly SY (2007) Resetting of the U-Pb zircon system in Cambro-Ordovician intrusives of the Deep Freeze Range, Northern Victoria Land Antarctica. J Petrol 48(2):327–364

Bonin B, Brändlein P, Bussy F, Desmons J, Eggenberger U, Finger F, Graf K, Marro C, Mercolli I, Oberhänsli R, Ploquin A, von Quadt A, von Raumer JF, Schaltegger U, Streyrer HP, Visonà D, Vivier G (1993) Late Variscan magmatic evolution of the Alpine basement. In: von Raumer JF, Neubauer F (eds) Pre-Mesozoic geology in the Alps. Springer, Berlin, pp 171–201

Bussien D, Bussy F, Magna T, Masson H (2011) Timing of Palaeozoic magmatism in the Maggia and Sambuco nappes and paleogeographic implications (Central Lepontine Alps). Swiss J Geosci 104(1):1–29

Bussy F, Derron MH, Jacquod J, Sartori M, Thélin P (1996) The 500 Ma-old Thyon metagranite: a new A-type granite occurrence in the western Penninic Alps (Wallis, Switzerland). Eur J Mineral 8:565–575

Bussy F, Hernandez J, von Raumer JF (2000) Bimodal magmatism as a consequence of the post-collisional readjustment of the thickened Variscan continental lithosphere (Aiguilles Rouges - Mont Blanc Massifs, Western Alps). Geological Society of America Special Papers 350:221–233

Corfu F, Hanchar JM, Hoskin PWO, Kinny P (2003) Atlas of zircon textures. In: Hanchar JM, Hoskin PWO (eds) Reviews in mineralogy and geochemistry, vol 53., zirconMineral Society of America, Washington, pp 469–500

Dickin AP (1988) Evidence for limited REE leaching from the Roffna Gneiss, Switzerland—a discussion of the paper by Vocke et al. (1987) (CMP95:145–154). Contrib Miner Petrol 99 (2):273–275

Díez Fernández R, Castiñeiras P, Gómez Barreiro J (2012) Age constraints on Lower Paleozoic convection system: magmatic events in the NW Iberian Gondwana margin. Gondwana Res 21(4):1066–1079

Eichhorn R, Loth G, Höll R, Finger F, Schermaier A, Kennedy A (2000) Multistage Variscan magmatism in the central Tauern window (Austria) unveiled by U/Pb SHRIMP zircon data. Contrib Miner Petrol 139(4):418–435

Eisbacher GH, Lüschen E, Wickert F (1989) Crustal-scale thrusting and extension in the Hercynian Schwarzwald and Vosges, central Europe. Tectonics 8(1):1–21

Finger F, Roberts MP, Haunschmid B, Schermaier A, Steyrer HP (1997) Variscan granitoids of central Europe: their typology, potential sources and tectonothermal relations. Mineral Petrol 61(1):67–96

Franke W (2006) The Variscan orogen in Central Europe: construction and collapse. Geological Society, London, Memoirs 32(1):333–343

Galli A, Le Bayon B, Schmidt M, Burg JP, Reusser E, Sergeev S, Larionov A (2012) U-Pb zircon dating of the Gruf Complex: disclosing the late Variscan granulitic lower crust of Europe stranded in the Central Alps. Contrib Miner Petrol 163(2): 353–378

Ganzfried R (1984) Geologisch-petrographische Untersuchungen im SE-Rand der Suretta-Decke im hinteren Val da Roda. University of Bern, Diploma thesis

Grünenfelder M (1956) Petrographie des Roffnakristallins in Mittelbünden und seine Eisenvererzungen. Beiträge zur Geologie der Schweiz 35: 57

Guillot F, Schaltegger U, Bertrand J, Deloule É, Baudin T (2002) Zircon U-Pb geochronology of Ordovician magmatism in the polycyclic Ruitor Massif (Internal W Alps). Int J Earth Sci 91(6): 964–978

Gysin M (1963) Les feldspaths potassiques des porphyres de Roffna. Schweiz Mineral Petrogr Mitt 43(1):385–406

Hann HP, Chen F, Zedler H, Frisch W, Loeschke J (2003) The Rand Granite in the southern Schwarzwald and its geodynamic significance in the Variscan belt of SW Germany. Int J Earth Sci 92(6):821–842

Hanson GN, Grünenfelder M, Soptrayanova G (1969) The geochronology of a recrystallized tectonite in Switzerland: the Roffna gneiss. Earth Planet Sci Lett 5:413–422

Heim A (1891) Das Thalgebiet von Schams. Beiträge zur Geologischen Karte der Schweiz 25(10):377–407

Jackson SE, Pearson NJ, Griffin WL, Belousova EA (2004) The application of laser ablation-inductively coupled plasma-mass spectrometry to in situ U-Pb zircon geochronology. Chem Geol 211(1–2):47–69

Kooijman E, Berndt J, Mezger K (2012) U-Pb dating of zircon by laser ablation ICP-MS: recent improvements and new insights. Eur J Mineral 24(1):5–21

Korokovsky SP, Putis M, Kotov AB, Sal'nikova EB, Kovach VP (1998) High-pressure metamorphism of Phengite Gneisses in the Lower Austro-Alpine Nappe Unit, Eastern Alps: mineral equilibria, *P-T* parameters, and age. Petrology 6:655–672

Kroner U, Mansy J-L, Mazur S, Aleksandrowski P, Hann HP, Huckriede H, Lacquement F, Lamarche J, Ledru P, Pharaoh TC, Zedler H, Zeh A, Zulauf G (2008) Variscan tectonics. In: McCann T (ed) The geology of central Europe, vol 1., Precambrian and Palaeozoic. Geological Society, London, pp 599–664

Kryza R, Crowley QG, Larionov A, Pin C, Oberc-Dziedzic T, Mochnacka K (2012) Chemical abrasion applied to SHRIMP zircon geochronology: an example from the Variscan Karkonosze Granite (Sudetes, SW Poland). Gondwana Res 21(4): 757–767

Ludwig KR (2008) User's Manual for Isoplot 3.70. A Geochronological Toolkit for Microsoft Excel. Berkeley Geochron Center Spec Pub 4:76

Marotta AM, Spalla MI (2007) Permian-Triassic high thermal regime in the Alps: Result of late Variscan collapse or continental

rifting? Validation by numerical modeling. Tectonics 26 (4): TC4016
Marquer D, Challandes N, Baudin T (1996) Shear zone patterns and strain distribution at the scale of a Penninic nappe: the Suretta nappe (Eastern Swiss Alps). J Struct Geol 18(6):753–764
Marquer D, Challandes N, Schaltegger U (1998) Early Permian magmatism in Briançonnais terranes: Truzzo granite and Roffna rhyolite (eastern Penninic nappes, Swiss and Italian Alps). Schweiz Mineral Petrogr Mitt 78(3):397–414
Mattinson JM (2005) Zircon U-Pb chemical abrasion ("CA-TIMS") method: combined annealing and multi-step partial dissolution analysis for improved precision and accuracy of zircon ages. Chem Geol 220(1–2):47–66
Mayerat Demarne A-M (1994) Analyse structurale de la zone frontale de la nappe du Tambo (Pennique, Grisons, Suisse). Beiträge zur Geologischen Karte der Schweiz 165:168
Miller JS, Matzel JEP, Miller CF, Burgess SD, Miller RB (2007) Zircon growth and recycling during the assembly of large, composite arc plutons. J Volcanol Geoth Res 167(1–4):282–299
Milnes AG, Schmutz H-U (1978) Structure and history of the Suretta nappe (Pennine zone, Central Alps): a field study. Eclogae Geol Helv 71(1):19–33
Neubauer F (2002) Evolution of late Neoproterozoic to early Paleozoic tectonic elements in Central and Southeast European Alpine mountain belts: review and synthesis. Tectonophysics 352(1–2):87–103
Nussbaum C, Marquer D, Biino GG (1998) Two subduction events in a polycyclic basement: Alpine and pre-Alpine high-pressure metamorphism in the Suretta nappe, Swiss Eastern Alps. J Metamorph Geol 16(5):591–605
Oberc-Dziedzic T, Klimas K, Kryza R, Fanning CM (2003) SHRIMP U-Pb zircon geochronology of the Strzelin gneiss, SW Poland: evidence for a Neoproterozoic thermal event in the Fore-Sudetic Block, Central European Variscides. Int J Earth Sci 92(5):701–711
Oberhänsli R, Bousquet R, Engi M, Goffé B, Gosso G, Handy MR, Höck V, Koller F, Lardeaux J-M, Polino R, Rossi P, Schuster R, Schwartz S, Spalla I (2004) Metamorphic structure of the Alps. 1:1,000,000. sGMW, Paris
Pfiffner OA (1993) Palinspastic reconstruction of the pre-Triassic basement units in the Alps: the central Alps. In: von Raumer JF, Neubauer F (eds) Pre-Mesozoic geology in the Alps. Springer, Berlin, pp 29–39
Pin C, Kryza R, Oberc-Dziedzic T, Mazur S, Turniak K, Waldhausrová J (2007) The diversity and geodynamic significance of Late Cambrian (ca. 500 Ma) felsic anorogenic magmatism in the northern part of the Bohemian Massif: a review based on Sm-Nd isotope and geochemical data. Geological Society of America Special Papers 423:209–229
Ring U (1992) The Alpine geodynamic evolution of Penninic nappes in the eastern central Alps: geothermobarometric and kinematic data. J Metamorph Geol 10(1):33–53
Rüetschi G (1903) Zur Kenntnis des Roffnagesteines. Eclogae Geol Helv 8:5–45
Schaltegger U (1997) Magma pulses in the Central Variscan Belt: episodic melt generation and emplacement during lithospheric thinning. Terra Nova 9(5–6):242–245
Schaltegger U (2000) U-Pb geochronology of the Southern Black Forest Batholith (Central Variscan Belt): timing of exhumation and granite emplacement. Int J Earth Sci 88(4):814–828
Schaltegger U, Brack P (2007) Crustal-scale magmatic systems during intracontinental strike-slip tectonics: U, Pb and Hf isotopic constraints from Permian magmatic rocks of the Southern Alps. Int J Earth Sci 96(6):1131–1151
Schaltegger U, Gebauer D (1999) Pre-Alpine geochronology of the Central, Western and Southern Alps. Schweiz Mineral Petrogr Mitt 79(1):79–87
Schaltegger U, Nägler TF, Corfu F (1997) A Cambrian island arc in the Silvretta nappe: constraints from geochemistry and geochronology. Schweiz Mineral Petrogr Mitt 77(3):337–350
Schaltegger U, Albrecht J, Corfu F (2003) The Ordovician orogeny in the Alpine basement: constraints from geochronology and geochemistry in the Aar Massif (Central Alps). Schweiz Mineral Petrogr Mitt 83(2):183–195
Schaltegger U, Brack P, Ovtcharova M, Peytcheva I, Schoene B, Stracke A, Marocchi M, Bargossi GM (2009) Zircon and titanite recording 1.5 million years of magma accretion, crystallization and initial cooling in a composite pluton (southern Adamello batholith, northern Italy). Earth Planet Sci Lett 286(1–2):208–218
Scheiber T, Pfiffner OA, Schreurs G (2012) Strain accumulation during basal accretion in continental collision: a case study from the Suretta nappe (eastern Swiss Alps). Tectonophysics 579: 56–73
Schmid SM, Pfiffner OA, Schreurs G (1997) Rifting and collision in the Penninic zone of eastern Switzerland. In: Pfiffner OA, Lehner P, Heitzmann P, Mueller S, Steck (eds) A Deep Structure of the Swiss Alps: Results of NRP 20. Birkhäuser Verlag, pp 160–185
Schmid SM, Fügenschuh B, Kissling E, Schuster R (2004) Tectonic map and overall architecture of the Alpine orogen. Eclogae Geol Helv 97(1):93–117
Schmidt C (1891) Gesteine aus dem Thalgebiete von Schams. Beiträge zur Geologischen Karte der Schweiz 25:73–76
Schuster R, Stüwe K (2008) Permian metamorphic event in the Alps. Geology 36(8):603–606
Sircombe KN (2004) AgeDisplay: an EXCEL workbook to evaluate and display univariate geochronological data using binned frequency histograms and probability density distributions. Comput Geosci 30(1):21–31
Spicher A (1980) Tektonische Karte der Schweiz. 1:500,000. Bundesamt für Wasser und Geologie, Bern
Stacey JS, Kramers JD (1975) Approximation of terrestrial lead isotope evolution by a two-stage model. Earth Planet Sci Lett 26(2):207–221
Stampfli GM, Mosar J, Marquer D, Marchant R, Baudin T, Borel G (1998) Subduction and obduction processes in the Swiss Alps. Tectonophysics 296(1–2):159–204
Staub R (1926) Geologische Karte des Avers. 1:50.000 Geol. Spez. Karte 97. Schweiz Geol Komm
Steiger RH, Jäger E (1977) Subcommission on geochronology: convention on the use of decay constants in geo- and cosmochronology. Earth Planet Sci Lett 36(3):359–362
Steinitz G, Jäger E (1981) Rb-Sr and K-Ar studies on rocks from the Suretta nappe; Eastern Switzerland. Schweiz Mineral Petrogr Mitt 61:121–131
Streiff V, Jäckli H, Neher J (1971) Geologischer Atlas der Schweiz. 1:25.000 Blatt Andeer (Nr. 1235). Schweiz Geol Komm
Streiff V, Jäckli H, Neher J (1976) Erläuterungen zum Blatt 1235 Andeer des Geologischen Atlas der Schweiz 1:25.000. Schweiz Geol Komm
Thélin P, Sartori M, Burri M, Gouffon Y, Chessex R (1993) The pre-Alpine basement of the Briançonnais (Wallis, Switzerland). In: von Raumer JF, Neubauer F (eds) Pre-Mesozoic geology in the Alps. Springer, Berlin, pp 297–315
Timmerman MJ (2008) Palaeozoic magmatism. In: McCann T (ed) The geology of central Europe, vol 1., Precambrian and Palaeozoic. Geological Society, London, pp 665–748
Vocke RD, Hanson GN, Grünenfelder M (1987) Rare earth element mobility in the Roffna Gneiss, Switzerland. Contrib Mineral Petrol 95(2):145–154
von Raumer J, Stampfli GM, Borel G, Bussy F (2002) Organization of pre-Variscan basement areas at the north-Gondwanan margin. Int J Earth Sci 91(1):35–52

von Raumer JF, Stampfli GM, Bussy F (2003) Gondwana-derived microcontinents—the constituents of the Variscan and Alpine collisional orogens. Tectonophysics 365(1–4):7–22

von Raumer J, Bussy F, Stampfli GM (2009) The Variscan evolution in the External massifs of the Alps and place in their Variscan framework. CR Geosci 341(2–3):239–252

Wayne DM, Sinha AK (1992) Stability of Zircon U-Pb Systematics in a Greenschist-Grade Mylonite: an example from the Rockfish Valley Fault Zone, Central Virginia USA. J Geol 100(5):593–603

Wiedenbeck M, Allé P, Corfu F, Griffin WL, Meier M, Oberli F, von Quadt A, Roddick JC, Spiegel W (1995) Three natural zircon standards for U-Th-Pb, Lu-Hf, trace element and REE analyses. Geostand Newslett 19:1–23

Wiedenbeck M, Hanchar JM, Peck WH, Sylvester P, Valley J, Whitehouse M, Kronz A, Morishita Y, Nasdala L, Fiebig J, Franchi I, Girard J-P, Greeenwood RC, Hinton R, Kita N, Mason PRD, Norman M, Ogasawara M, Piccoli PM, Rhede D, Satoh H, Schulz-Dobrick B, Skår Ø, Spicuzza MJ, Terada K, Tindle K, Togashi S, Vennemann T, Xie Q, Zheng YF (2004) Further characterisation of the 91500 zircon crystal. Geostand Geoanal Res 28(1):9–39

Wiederkehr M (2004) Strukturelle und metamorphe Entwicklung der Metasedimente am Kontakt Briançonnais—Piemont-Liguria. University of Basel, Diploma thesis

Wilhelm O (1929) Geologie der Landschaft Schams. 1:50.000 Geol. Spez. Karte 114 (mit Profilen). Schweiz Geol Komm

Wilson M, Neumann E-R, Davies GR, Timmerman MJ, Heeremans M, Larsen BT (2004) Permo-Carboniferous magmatism and rifting in Europe: introduction. Geological Society, London, Special Publications 223:1–10